A brief study concerning thermal transport properties of B-C-N monolayers and graphene/X nanoribbon heterojunctions: Influences of carbon concentration and mean temperature

G. Cuba-Supanta[a,b,*], M. Martinez[b], C. Rojas-Ayala[b], and J. Rojas-Tapia[b]
[a]*Departamento Académico de Física, Facultad de Ciencias Naturales y Matemática, Universidad Nacional del Callao, Av. Juan Pablo II 306, Bellavista 07011, Callao, Perú.*
[*]*e-mail: gcubas@unac.edu.pe*
[b]*Grupo de Métodos Computacionales Aplicados a Nanomateriales, Facultad de Ciencias Físicas, Universidad Nacional Mayor de San Marcos, Apartado Postal 14-0149, Lima 14, Perú.*

Received 19 September 2024; accepted 4 May 2026

A wide variety of two-dimensional (2D) materials provides an optional route for manipulating heat fluxes at the nanoscale. Nowadays, 2D carbon-based materials have received important attention due to their adjustable transport properties by a controlled tuning of composition, junction, geometry, etc. In the present paper, we address the thermal transport properties of the B-C-N (Boron-Carbon-Nitride) monolayers and graphene/X (X=hBN, hSiC, and graphane) nanoribbon heterojunctions by performing non-equilibrium molecular dynamics simulations. Our results show that the carbon concentration modifies the thermal conductivity of B-C-N monolayers at a mean temperature of 300 K, producing values of 29.47, 28.94, and 16.58 W/m-K for concentrations of 90, 10, and 50%, respectively. Nevertheless, no major effect of carbon concentration on the temperature profile of B-C-N monolayers is observed. On the other hand, the mean temperature influences the interface thermal resistance and thermal conductivity of coplanar graphene/X nanoribbon heterojunctions, these variations are observed for the forward direction of the heat flux, modulating the temperature drop at the interface. Besides, graphene/hBN and graphene/graphane heterojunctions show a pronounced thermal rectification at a mean temperature below 300 K, compared to graphene/hSiC heterojunction. In which the heat fluxes present an asymmetry in the $j - \Delta$ curve, highlighting that the heat flux in the backward direction preferentially flows from X (hBN and graphane) to graphene nanoribbons.

Keywords: B-C-N monolayers; graphene-based nanoribbon heterojunctions; thermal transport properties; NEMD simulations.

DOI: https://doi.org/10.31349/RevMexFis.72.051001

1. Introduction

Since the discovery of graphene (2004), the family of two-dimensional (2D) honeycomb lattice materials has expanded rapidly. As a result several 2D materials have been fabricated and extensively studied, such as hexagonal boron nitride (hBN) [1], transition metal dichalcogenides (MoS_2 and WS_2) [2], transition metal carbides and nitrides (MXenes) [3], and a few others [4,5]. The significance of 2D materials is associated with their relevant and novel physicochemical properties that depend mainly on their structure, size, chirality, and composition. These aspects make them useful for the development of new technologies such as thermal-electronic devices, sensors, and energy storage, among other applications [1-5], unlike the zero band gap (Dirac cone) of graphene.

In order to address the next-generation thermal-management materials, it is important to explore novel 2D materials that are candidates to solve certain limitations of current technology. As is well known, the hBN and graphene are similar and comparable systems in some aspects (there are also many differences), *i.e.*, mechanical properties, thermal response, covalent bonds with sp^2 hybridization, low mass density, etc [6,7]. Currently, hexagonal boron carbon nitrides (hBCNs) are a new group of 2D structures consisting mainly of complex materials including B-C, C-N, B-N, and C-C bonds [6,8,9]. The stoichiometry-dependent properties of hBCNs, as well as the difficult-to-control domain distribution (between B, N, and C atoms), create challenges for device fabrication with efficient and reproducible performance [10-12]. In addition, by exploring the B-C-N ternary phase diagram, it is possible to indicate stable phases, where some physical properties of different monolayers such as BCN, BC_2N, and BC_4N are being determined [6,13,14]. Likewise, these structures are being applied in a wide range of fields, including supercapacitors and lithium-ion batteries to electrocatalysts and sensors [6,15]. Therefore, constant monitoring of the chemical proportions in hBCNs is a challenge in relation to the final composition that can deviate from B/C/N=1:1:1 [8].

In the same line of research, other 2D material heterojunctions, such as thermal diodes, are promising candidates for future cooling technologies. The main application of heat sinks, as a type of thermal interface material, is passive cooling, which is particularly attractive when the size of the electronic device to be cooled is taken into account. In addition, this type of cooling is economical and does not require maintenance or consume additional energy [7]. In fact, the graphene-based heterojunctions consist of graphene and other 2D materials in vertical and horizontal coupling;

this additional diversity can enhance the thermal transport properties. For example, several 2D heterojunctions, such as graphene/: hBN [16-19], silicene [20,21], MoS_2 [16,22], graphane [23,24], and black phosphorene [25], have been studied in both simulation and experimental works. Besides, over the last two decades, emerging 2D materials have been explored to manipulate interfacial thermal conductance, thermal conductivity, and thermal rectification ratio [7,26,27].

In this article, we report the thermal transport properties of B-C-N monolayers and coplanar graphene/X (X=hBN, hSiC, and graphane) nanoribbon heterojunctions under the influence of carbon concentration and the effect of mean temperature. We have performed non-equilibrium molecular dynamics simulations for this study. In the next section, we describe simulation details and methods, and then proceed to discuss the results, which are divided into two subsections. Finally, in the last section, our conclusions are summarized.

2. Computational details and methodology

The simulations were carried out using the non-equilibrium molecular dynamics (NEMD) method implemented in the LAMMPS code [28]. The standard velocity Verlet algorithm was used to integrate Newton's equations of motion, and the molecular dynamic time step was set to 0.1 fs. Before the NEMD simulations, all investigated systems were initially relaxed using the conjugate method to optimize the structures (relaxation time equal to 0.1 ps). Then, for each mean temperature, T_0, the equilibration runs for 5 ns considering an NVT ensemble (canonical ensemble) with a Nosé-Hoover thermostat. Once the temperature reached the required value, the thermostat was removed, and the NEMD simulations were carried out for 20 ns. Furthermore, the temperatures for left and right heat baths were defined as $T_L = (1+\Delta)T_0$ and $T_R = (1-\Delta)T_0$ (see Fig. 1), where heat flux flows left-to-right for the forward direction and right-to-left for the backward direction. Also, we considered a temperature bias of $\Gamma = |T_L - T_R| = 2\Delta T_0$ (Δ parameter varies from 0.01 to 0.5). Additionally, to avoid spurious effects associated with the specific choice of velocities (related to temperature), an average of five random choices of the initial velocity distribution was additionally performed.

As a matter of fact, the computational details mentioned are valid for the two graphitic systems studied: B-C-N monolayers and coplanar graphene/X (X=hBN, hSiC, and graphane) nanoribbon heterojunctions. It is worth mentioning that hSiC is a 2D silicon carbide with a hexagonal and planar structure [29]. On the one hand, the interactions among B, C, and N atoms for B-C-N monolayers were simulated by using an optimized Tersoff force field parametrized by Kinaci *et al.* [30], which has been widely used for the investigation of the physical properties of various BCN nanomaterials [17,19,31]. On the other hand, we have used three force fields for graphene/X nanoribbon heterojunctions as follows: X=hBN (hexagonal boron nitride), X=hSiC (siligraphene 1:1), and X=graphane (hydrogenated graphene) were simulated using the optimized Tersoff potential by Kinaci *et al.* [30], the many-body potential proposed by Tersoff [32], and the adaptive intermolecular reactive bond order (AIREBO) potential provided by Stuart *et al.* [33], respectively.

In order to quantify the thermal transport properties, the temperature profile was first computed by dividing the graphitic system into a certain number of slabs and using the relation [18,34]:

$$T_i = \frac{1}{3N_i k_B}\sum_{a=1}^{N_i}\langle m_a v_a^2\rangle, \tag{1}$$

where N_i is the number of atoms in the i-th slab, and m_a and v_a correspond to the mass and velocity of atom-a. Moreover, the calculated temperature for each slab (T_i) was averaged over a time interval to obtain a smooth temperature profile. The next quantity calculated was the thermal conductivity, κ, which is the heat conduction ability along graphitic systems and for graphene/X heterojunctions can be calculated by a mixture rule-based expression, which has been successfully used to study hybrid monolayers [20]:

$$\kappa^{-1} = \frac{1}{2}\kappa_g^{-1} + \frac{1}{2}\kappa_X^{-1} + \frac{1}{L}G^{-1}, \tag{2}$$

where κ_g and κ_X are the thermal conductivities of graphene and X nanoribbons, respectively. The $\kappa_X = jL/A|T_L - T_R|$ (valid for B-C-N monolayers) comes from Fourier's law of heat conduction. The G is the thermal conductance, $G = R_K^{-1}$, which comes from calculating the interface thermal resistance (called Kapitza resistance) between graphene and X nanoribbons at the interface, $R_K = A\Delta T/j$. In addition, $A = W \times h$ ($h = 0.33$ nm) is the cross-sectional area that the heat flux passes through, and ΔT is the temperature drop across the interface.

Another important phenomenon is the thermal rectification, η, which appears when the heat flux is different in the reverse direction [17,19,26,35]. Therefore, the thermal rectification is defined as $\eta(\%) = |(j_+/j_-) - 1| \times 100$, where the heat fluxes $j_{+,-}$ indicate whether the graphene/X nanoribbon heterojunction is operated in the forward or backward direction. The $j_{+,-}$ induced by the temperature bias Γ are computed as $j_{+,-} = (\partial E_L^{+,-}/\partial t + \partial E_R^{+,-}/\partial t)/2$, where $E_L^{+,-}$ and $E_R^{+,-}$ are the total energies that have been added to/subtracted from the atoms in the hot/cold regions for temperature control, respectively.

3. Results and discussion

3.1. B-C-N monolayers: Influences of carbon concentration and mean temperature

We first analyzed the thermal transport properties of B-C-N monolayers using average quantities such as thermal conductivity and temperature profile, where we only focused on the forward direction of heat flux. Following the experimental

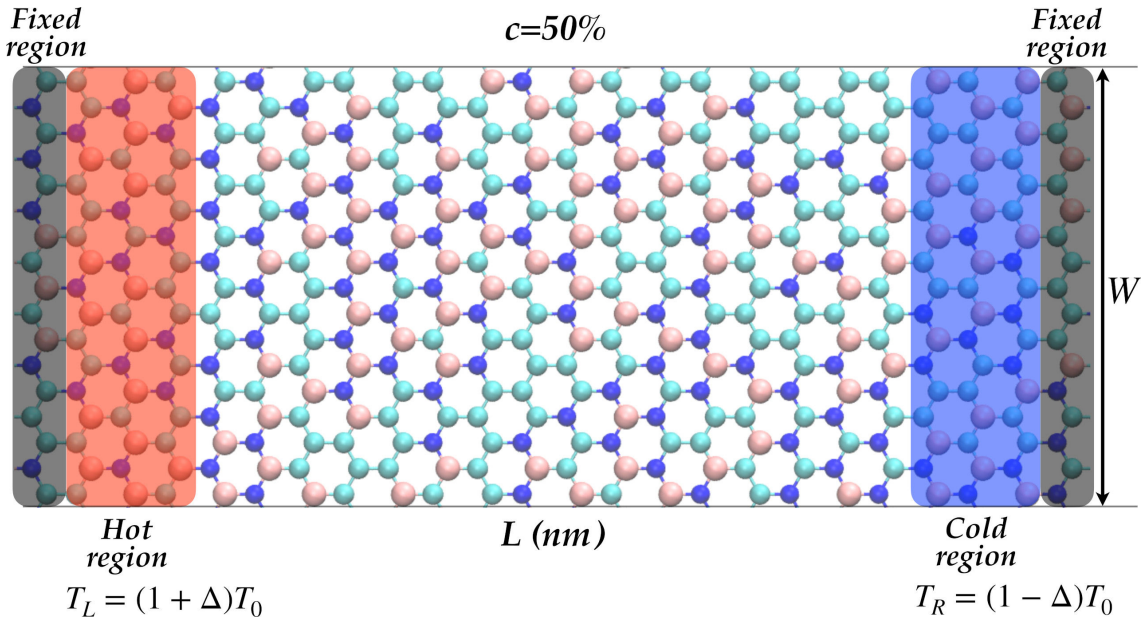

FIGURE 1. Schematic representation of thermal transport setup for B-C-N monolayer at 50% of carbon concentration. For all concentrations, the dimensions are $L \approx 13$ nm, $W \approx 7.3$ nm, and the hot or cold region ≈ 3.3 nm. The pink, cyan, and blue balls correspond to the B, C, and N atoms, respectively.

study on h-BCN by Beniwal *et al.* [8] and theoretical works by Zhang *at al.* [31,36], we have considered a model based on a random carbon substitution in h-BN as an alternative proposal for a different atomic ratio of B/C/N. The carbon concentration was defined as $c = (N_C/N)100\%$, where N_C is the number of carbon atoms, and N is the total number of atoms, maintaining the same number of B and N atoms. For example, the atomic ratio with the concentration of 50% is B/C/N=1:2:1. In Fig. 1, the illustrative model for NEMD of thermal transport at $c = 50\%$ is shown. We have fixed the ends in the X-direction (fixed region) to avoid global rotations of the system during the simulation. Also, we have considered periodic boundary conditions on the XY plane for all carbon concentrations of B-C-N monolayers.

The thermal conductivity of B-C-N monolayers as a function of carbon concentration is shown in Fig. 2a). The thermal conductivities present large values of 28.94 and 29.47 $W/m-K$ for concentrations of 10% and 90%, respectively, and a small value of 16.58 W/m-K for the concentration around 50%. The κ values are similar to h-BCN systems close in the atomic ratio [36], these values are very small compared to the pristine graphene and hBN systems. Meanwhile, the experimental thermal conductivity of the BCN nanosheets exhibited a relatively low value (0.58-1.86 W/mK) [10]; however, aligned carbon doping in hBCN thin films can improve heat transport (836 ± 312 W/mK) [37]. In our work it is clearly observed that the values of κ depend strongly on the heat flux [see inset of Fig. 2a)] that manages to pass through the monolayer with a certain carbon concentration. In the meantime, we can observe in Fig. 2b) that the temperature profile for the forward direction gradually decreases along the B-C-N monolayers (L). This decrease in temperature throughout the transport device occurs for different carbon concentrations corresponding to a thermal bath of T_L =330 K (the first three points on the left) and $T_R = 270$ K (the last three points on the right) with a temperature bias of $\Gamma = 60$ K. The relationships between T and L are practically linear and quasi-independent of the carbon concentration. Furthermore, this trend is observed for other high values of mean temperature (data not shown), which suggests that these B-N-C monolayers can be used as thermal devices that operate at high temperatures without losing their sensitivity.

Likewise, the influence of mean temperature on the thermal conductivities and temperature profiles of B-C-N monolayers for a temperature bias of $0.2 \times T_0$ is shown in Fig. 3. The κ values of the three concentrations increase as the T_0 increases, the gradual increase being monotonic for any concentration, resulting in values of 23.89, 18.08, and 24.70 W/m-K at 700 K for 20, 50, and 80%, respectively [see Fig. 3a)]. This marked dependence is mainly due to the significant increase in the heat flux provided by the thermal bath throughout the monolayer (see the inset box). For example, for $T_0 = 200$, 400, and 600 K, we have the temperature bias of 40, 80, and 120 K, respectively. Indeed, the value of heat fluxes is due to the majority or minority contribution of the B, N, and C atoms in the monolayer. However, for the 50% concentration, it is observed that the values of κ are always lower than the rest of the concentrations (20% and 80%). This characteristic is consistent with the κ in graph Fig. 2a) for c=50%. Consequently, in Fig. 3b), no significant influence of the T_0 on the temperature profile for the forward direction is observed, *i.e.*, all $T(K)$ show practically a linear and decreasing dependence along the B-C-N monolayer (L)

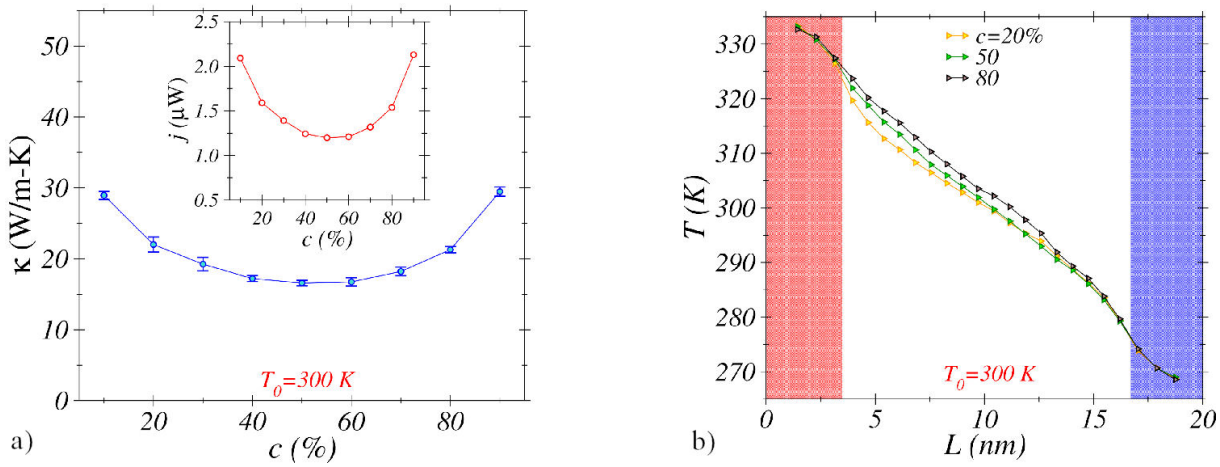

FIGURE 2. a) The thermal conductivity and the heat flux (inset box) of the B-C-N monolayer as a function of carbon concentration. b) Temperature profiles concerning the length of the system for carbon concentrations of 20%, 50%, and 80%. Both graphs at a mean temperature of 300 K and for $\Delta = 0.1$.

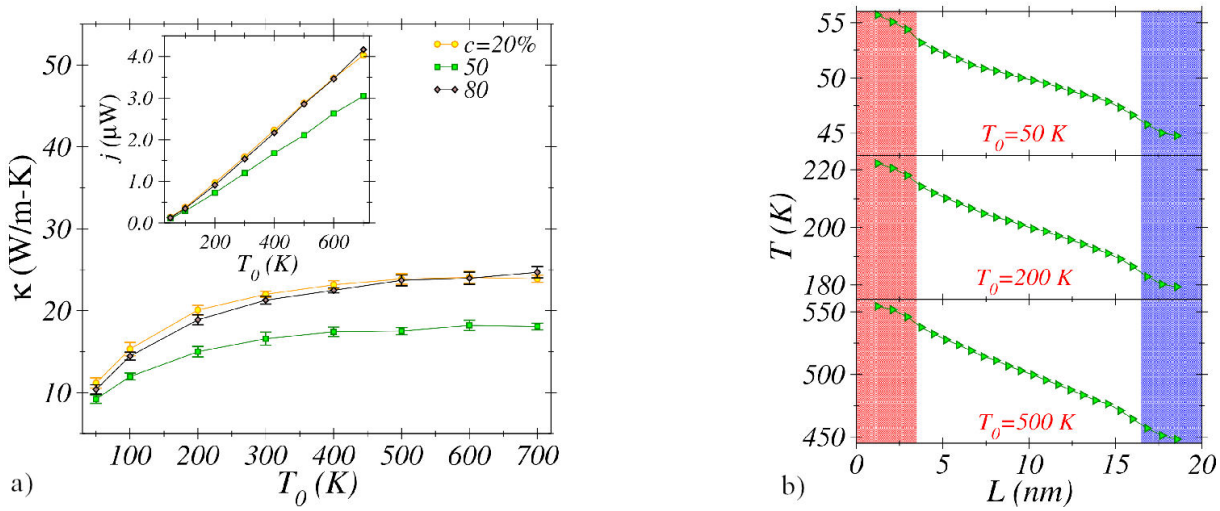

FIGURE 3. a) Thermal conductivities and heat fluxes (inset box) versus mean temperature of the B-C-N monolayers for carbon concentrations of 20%, 50%, and 80%. b) Temperature profiles concerning the length of the system for three values of the mean temperature at 50% of carbon concentration and for $\Delta = 0.1$.

for a fixed carbon concentration. This thermal response of the B-C-N monolayers is independent of the temperature bias of 10, 40, and 100 K, at $T_0 = 50$, 200, and 500 K, respectively.

3.2. Graphene/X nanoribbon heterojunctions: Effect of mean temperature

In this subsection, we proceed to study the dependence of mean temperature on the thermal transport properties of coplanar graphene/X (X=hBN, hSiC, and graphane) nanoribbon heterojunctions using the average quantities such as thermal conductivity, temperature profile, interface thermal resistance, thermal rectification, and $j - \Delta$ curve (corresponding to the $I - V$ curve for an electric rectifier). The setups of the thermal transport of graphene/X heterojunctions are shown in Fig. 4, where fixed regions, thermal baths, and the zigzag interface are observed. At the interface, C-N, C-C, and C-C bonds are formed for X=hBN, hSiC, and the graphane, respectively. After structural relaxation, the average bond lengths were 1.45 (B-N), 1.78 (Si-C), and 1.1 (C-H) Å, which are different from the bond length of graphene 1.42 Å. All simulations for free-standing heterojunctions have been done with free boundary conditions in all directions.

Once the graphene/X heterojunction reaches a thermal steady state, a heat flux is imposed along the entire device length ($L_G + L_X$), and the temperature profile is computed. Figure 5a) shows the temperature profile along the graphene to X nanoribbons (forward direction, j_+) at a mean temperature of 300 K and a temperature bias of 60 K. It is worth mentioning that in the NEMD simulation, the total energies of hot and cold regions are changing continuously, thus these regions are excluded from the thermal quantities calculations. The temperature variations in graphene/X hetero-

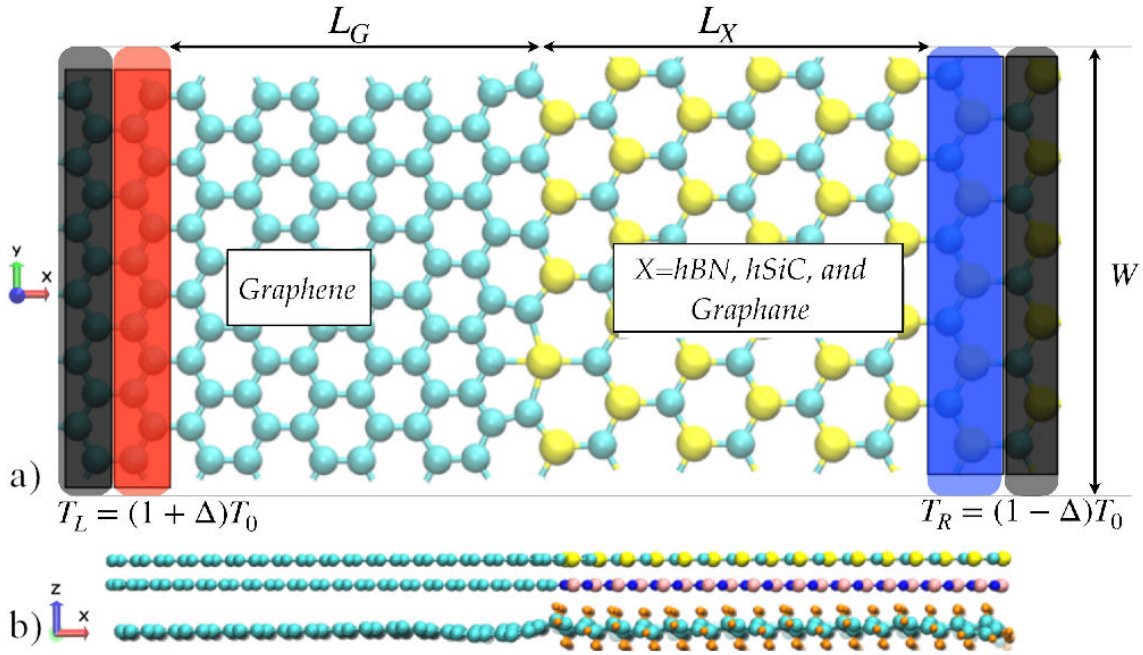

FIGURE 4. a) Schematic representation of thermal transport setup for the coplanar graphene/hSiC nanoribbon heterojunction from a top view. b) Atomic configuration of coplanar graphene/X (X=hSiC, hBN, and graphane) nanoribbon heterojunctions from a frontal view. For all heterojunctions, the dimensions are $L_G + L_X \approx 6$ nm, $W \approx 4.5$ nm, and the hot or cold region ≈ 1.5 nm. The cyan, yellow, pink, blue, and orange balls correspond to the C, Si, B, N, and H atoms, respectively.

junctions and the temperature drops at the interface are observed in these temperature profiles. This temperature drop (ΔT) is used to calculate the thermal resistance, indicating that the interface plays a crucial role in controlling or enhancing thermal transport in different heterojunctions. The noticeable change in temperature drop at the heat bath-device interface is $\Delta T \sim 24$ K (for X=hBN) compared to $\Delta T \sim 16$ K (for hSiC) or $\Delta T \sim 12$ K (for graphane).

For the forward direction, the interface thermal resistance, R_K, is reduced according to the mean temperature increase independently of material heterojunction [see Fig. 5b)]. To our knowledge, the R_K is usually lower as the temperature is higher [16,18]. Moreover, this decrease in the R_K values is directly associated with a small ΔT and big heat flux from the graphene to the other nanoribbon, *i.e.*, as the mean temperature increases, the heat flux passes through the device with a lower opposition at the interface. Various experimental techniques were used to measure the thermal contact resistance in different graphene-based nanomaterials; the works report higher orders of R_K [27,38]. Interestingly, our results are in contrast to those found for thermal conductivities, which gradually increase as a function of the mean temperature, reaching a maximum value of 106 W/m-K at 700 K for the graphene/hBN heterojunction compared to graphene/graphane heterojunction (61 W/m-K).

For the sake of clarity, we now focus on the forward and backward directions of the heat flux (j_+ and j_-) to analyze the thermal rectification, η. As seen in Fig. 6a), the η(%) displays a non-monotonous dependence with respect to the mean temperature, where for high T_0 a minimum at the crossing point of the forward and backward heat fluxes is observed. The η can reach values up to ∼86%, 67%, and 27% when the mean temperature is 50 K for X=hBN, graphane, and hSiC, respectively. Furthermore, the gradual decrease of η is mainly because the forward and backward heat fluxes are similar. For the graphene/hBN heterojunction, the value $j_+ \equiv j_-$ is at temperatures greater than 400 K [see inset of Fig. 6a)]. The heat flux in the backward direction from hBN towards graphene nanoribbon heterojunction is always greater than in the forward direction ($j_- > j_+$), in which an asymmetry in the heat flux is predicted; the results for thermal rectification and heat flux are in agreement with previously published theoretical and experimental work [17,26,39].

In order to test the prediction above, we present the heat flux versus the Δ parameter at room temperature in Fig. 6b). In general, the relationship between j and Δ is indeed asymmetric with respect to $\Delta = 0$ for two graphene/X heterojunctions. We first analyze the graphene/hBN heterojunction, when $\Delta < 0$, the heat flux ($j_{hBN\to G}$) increases rapidly with Δ, meanwhile for $\Delta > 0$, the heat flux ($j_{G\to hBN}$) is much smaller and presents a negative differential thermal resistance (NDTR) at $\Delta = 0.5$, akin to that of other studies [17,40]. This effect on negative differential resistance was also observed in CNTs connected with BNNTs at high bias voltages [41]. Likewise, the graphene/graphane heterojunction also presents an asymmetry with respect to $\Delta = 0$, *i.e.*, the heat flux is greater/lesser for $\Delta < 0/\Delta > 0$. Obviously, this phenomenology is not clearly observed for the graphene/hSiC heterojunction. Therefore, the heat fluxes preferentially flow

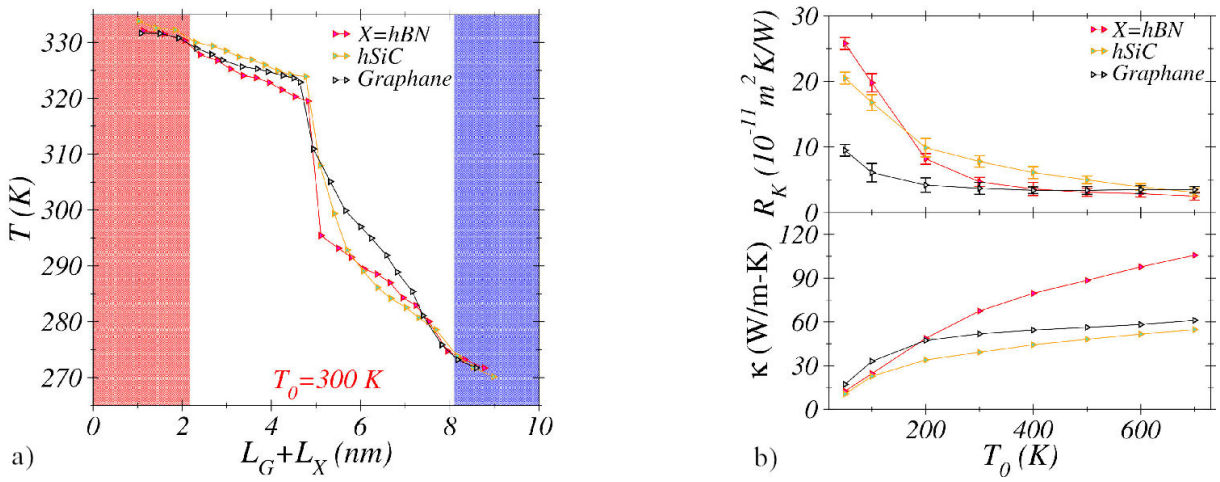

FIGURE 5. a) Temperature profiles concerning the device length for coplanar graphene/X nanoribbon heterojunctions. b) Interface thermal resistances and thermal conductivities as a function of the mean temperature of graphene/X nanoribbon heterojunctions. Both graphs are for the forward direction of the heat flux and Δ =0.1.

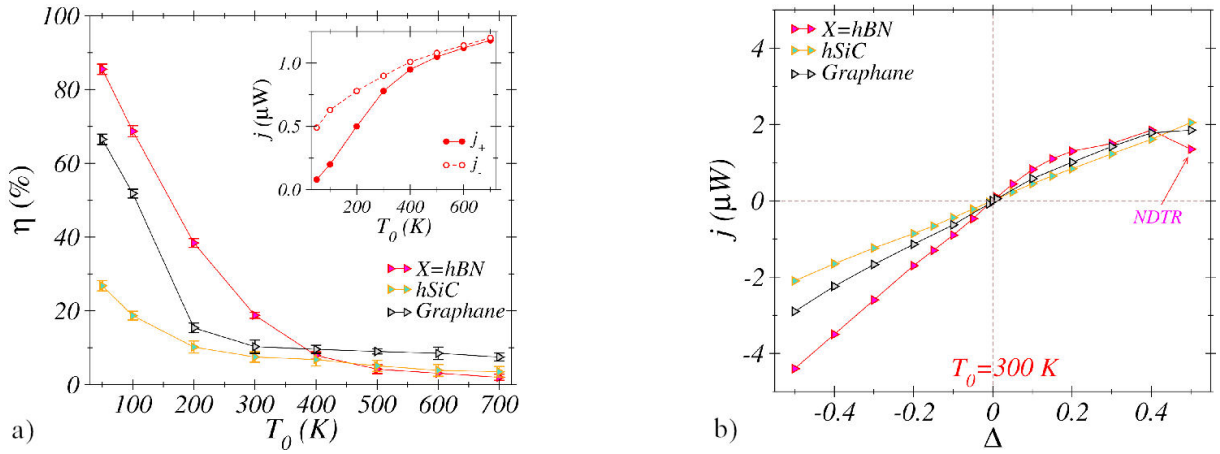

FIGURE 6. a) Thermal rectifications as a function of the mean temperature for graphene/X nanoribbon heterojunctions. Inset: heat fluxes in the forward and backward directions only for graphene/hBN heterojunction. b) The $j - \Delta$ curve (heat fluxes versus Δ parameter) for graphene/X nanoribbon heterojunctions at the mean temperature of 300 K.

from the X (hBN and graphane) to the graphene domain, which demonstrates a pronounced thermal rectification effect in these coplanar nanoribbon heterojunctions.

4. Conclusions

In this study, the influences of carbon concentration and mean temperature of B-C-N monolayers and coplanar graphene/X (X=hBN, hSiC, and graphane) nanoribbon heterojunctions were achieved by the use of molecular dynamics simulations. On the one hand, we have concluded that the carbon concentration modifies the thermal conductivity of B-C-N monolayers, generating various values at a mean temperature of 300 K, such as 29.47, 28.94, and 16.58 W/m-K for carbon concentrations of 90, 10, and 50%, respectively. Otherwise, no major effect of the carbon concentration on the temperature profile of B-C-N monolayers is observed. Likewise, when considering the increase in mean temperature, the thermal conductivity increases similarly for any concentration (except to a lesser extent for the 50%).

On the other hand, we also observed that the mean temperature influences the transport properties of coplanar graphene/X nanoribbon heterojunctions, namely, the interface thermal resistance decreases, and the thermal conductivity increases as the mean temperature increases for the forward direction of the heat flux. These variations were mainly due to the fact that the temperature drop (ΔT) observed in the temperature profile decreases, and the heat flux increases for increasingly larger thermal baths. Furthermore, the thermal rectification shows that graphene/hBN and graphene/graphane heterojunctions are good rectifiers at mean temperatures below 300 K, compared to graphene/hSiC heterojunction, because the rectification decreases as the mean temperature increases ($T_0 > 300$). This fact of pronounced rectification was corroborated in the $j - \Delta$ curve, in which there is an asymmetry in the heat flux with respect

to $\Delta = 0$ for these two heterojunctions, indicating that the heat flux preferentially flows from X (hBN and graphane) to graphene nanoribbons in heterojunctions.

Acknowledgements

All simulations were performed in the Workstations of the "Grupo de métodos computacionales aplicados a nanomateriales", Faculty of Physical Science, Universidad Nacional Mayor de San Marcos (UNMSM). J.R.T. thanks UNMSM for the financial support under RR N° 01686-R-20 and project number B20130811.

Conflicts of interest

The authors declare that they have no conflicts of interest.

1. V. Sharma *et al.*, Thermal transport properties of boron nitride based materials: *A review, Renewable and Sustainable Energy Reviews* **120** (2020) 109622, https://doi.org/10.1016/j.rser.2019.109622
2. D. Gupta, V. Chauhan, and R. Kumar, A comprehensive review on synthesis and applications of molybdenum disulfide (MoS2) material: Past and recent developments, *Inorganic Chemistry Communications* **121** (2020) 108200, https://doi.org/10.1016/j.inoche.2020.108200
3. T. Rasheed, MXenes as an emerging class of two-dimensional materials for advanced energy storage devices, *Journal of Materials Chemistry A* **10** (2022) 4558, https://doi.org/10.1039/D1TA10083A
4. M. Tahir *et al.*, A review on the 2D black phosphorus materials for energy applications, *Inorganic Chemistry Communications* **124** (2021) 108242, https://doi.org/10.1016/j.inoche.2020.108242
5. N. R. Glavin *et al.*, Emerging applications of elemental 2D materials, *Advanced Materials* **32** (2020) 1904302, https://doi.org/10.1002/adma.201904302
6. S. Angizi *et al.*, Two-dimensional boron carbon nitride: a comprehensive review, *ECS Journal of Solid State Science and Technology* **9** (2020) 083004, https://doi.org/10.1149/2162-8777/abb8ef
7. F. Wu *et al.*, High thermal conductivity 2D materials: From theory and engineering to applications, *Advanced Materials Interfaces* **9** (2022) 2200409, https://doi.org/10.1002/admi.202200409
8. S. Beniwal *et al.*, Graphene-like boron-carbon-nitrogen monolayers, *ACS nano* **11** (2017) 2486, https://doi.org/10.1021/acsnano.6b08136
9. L. Cheng *et al.*, Two-dimensional hexagonal boron-carbon- nitrogen atomic layers, *Nanoscale* **11** (2019) 10454, https://doi.org/10.1039/C9NR00712A
10. R. Attri *et al.*, Low thermal conductivity of 2D borocarbonitride nanosheets, *Journal of Solid State Chemistry* **282** (2020) 121105, https://doi.org/10.1016/j.jssc.2019.121105
11. S. Nappini *et al.*, Chemical composition and interaction strength of two-dimensional boron-nitrogen-carbon heterostructures driven by polycrystalline metallic surfaces, *Applied Surface Science* **479** (2019) 903, https://doi.org/10.1016/j.apsusc.2019.01.274
12. F. Leardini *et al.*, A fast synthesis route of boron-carbon-nitrogen ultrathin layers towards highly mixed ternary B-C-N phases, *2D Materials* **6** (2019) 035015, https://doi.org/10.1088/2053-1583/ab175c
13. S. Thomas and S. U. Lee, Atomistic insights into the anisotropic mechanical properties and role of ripples on the thermal expansion of h-BCN monolayers, *RSC advances* **9** (2019) 1238, https://doi.org/10.1039/C8RA08076C
14. L. Jiao *et al.*, Electronic, elastic, and optical properties of monolayer BC2N, *Journal of Solid State Chemistry* **244** (2016) 120, https://doi.org/10.1016/j.jssc.2016.09.012
15. M. Kaur *et al.*, Recent insights into BCN nanomaterials- synthesis, properties and applications, *New Journal of Chemistry* **47** (2023) 2137, https://doi.org/10.1039/D2NJ04763B
16. Z. Zhang *et al.*, Thermal transport in MoS2/Graphene hybrid nanosheets, *Nanotechnology* **26** (2015) 375402, https://doi.org/10.1088/0957-4484/26/37/375402
17. X.-K. Chen *et al.*, Thermal rectification and negative differential thermal resistance behaviors in graphene/hexagonal boron nitride heterojunction, *Carbon* **100** (2016) 492, https://doi.org/10.1016/j.carbon.2016.01.045
18. Y. Hong, J. Zhang, and X. C. Zeng, Thermal contact resistance across a linear heterojunction within a hybrid graphene/hexagonal boron nitride sheet, *Physical Chemistry Chemical Physics* **18** (2016) 24164, https://doi.org/10.1039/C6CP03933B
19. . L. M. Sandonas *et al.*, Enhancement of thermal transport properties of asymmetric Graphene/hBN nanoribbon heterojunctions by substrate engineering, *Carbon* **124** (2017) 642, https://doi.org/10.1016/j.carbon.2017.09.025
20. B. Liu *et al.*, Interface thermal conductance and rectification in hybrid graphene/silicene monolayer, *Carbon* **79** (2014) 236, https://doi.org/10.1016/j.carbon.2014.07.064
21. J. Zhou *et al.*, Phonon thermal transport in silicene/graphene heterobilayer nanostructures: Effect of interlayer interactions, *ACS omega* **7** (2022) 5844, https://doi.org/10.1021/acsomega.1c05932
22. X. Liu *et al.*, MoS 2-graphene in-plane contact for high interfacial thermal conduction, *Nano Research* **10** (2017) 2944, https://doi.org/10.1007/s12274-017-1504-8

23. A. Rajabpour, S. Vaez Allaei, and F. Kowsary, Interface thermal resistance and thermal rectification in hybrid graphenegraphane nanoribbons: A nonequilibrium molecular dynamics study, *Applied Physics Letters* **99** (2011), https://doi.org/10.1063/1.3622480

24. B. Liu *et al.*, Morphology and in-plane thermal conductivity of hybrid graphene sheets, *Applied Physics Letters* **101** (2012), https://doi.org/10.1063/1.4767388

25. Y.-Y. Zhang *et al.*, Interfacial thermal conductance in multilayer graphene/phosphorene heterostructure, *Journal of Physics D: Applied Physics* **49** (2016) 465301, https://doi.org/10.1088/0022-3727/49/46/465301

26. S. Zhao, Y. Zhou, and H. Wang, Review of thermal rectification experiments and theoretical calculations in 2D materials, *International Journal of Heat and Mass Transfer* **195** (2022) 123218, https://doi.org/10.1016/j.ijheatmasstransfer.2022.123218

27. W. Zheng *et al.*, Understanding and engineering interfacial thermal conductance of two-dimensional materials, *Surfaces and Interfaces* (2023) 103538, https://doi.org/10.1016/j.surfin.2023.103538

28. S. Plimpton, Fast Parallel Algorithms for Short-Range Molecular Dynamics, *Journal of Computational Physics* **117** (1995) 1, https://doi.org/10.1006/jcph.1995.1039

29. S. Chabi and K. Kadel, Two-dimensional silicon carbide: emerging direct band gap semiconductor, *Nanomaterials* **10** (2020) 2226, https://doi.org/10.3390/nano10112226

30. A. Kınacı*et al.*, Thermal conductivity of BN-C nanostructures, *Physical Review B* **86** (2012) 115410, https://doi.org/10.1103/PhysRevB.86.115410

31. Y.-Y. Zhang *et al.*, A molecular dynamics study of the mechanical properties of h-BCN monolayer using a modified Tersoff interatomic potential, *Physics Letters A* **383** (2019) 2821, https://doi.org/10.1016/j.physleta.2019.05.055

32. J. Tersoff, Modeling solid-state chemistry: Interatomic potentials for multicomponent systems, *Physical review B* **39** (1989) 5566, https://doi.org/10.1103/PhysRevB.39.5566

33. S. J. Stuart, A. B. Tutein, and J. A. Harrison, A reactive potential for hydrocarbons with intermolecular interactions, *The Journal of chemical physics* **112** (2000) 6472, https://doi.org/10.1063/1.481208

34. Q. Liang and Y. Wei, Molecular dynamics study on the thermal conductivity and thermal rectification in graphene with geometric variations of doped boron, *Physica B: Condensed Matter* **437** (2014) 36, https://doi.org/10.1016/j.physb.2013.12.035

35. F. K. Malik and K. Fobelets, A review of thermal rectification in solid-state devices, *Journal of Semiconductors* **43** (2022) 103101, https://doi.org/10.1088/1674-4926/43/10/103101 36.]

36. Y.-Y. Zhang *et al.*, Thermal conductivity of a h-BCN monolayer, *Physical Chemistry Chemical Physics* **19** (2017) 27326, https://doi.org/10.1039/C7CP04982J

37. P. R. Galligan *et al.*, Aligned carbon-doping to modulate thermal and electrical conductivity of boron carbon nitride grown from chemical vapor deposition, *Carbon* **215** (2023) 118397, https://doi.org/10.1016/j.carbon.2023.118397

38. Y. Xian *et al.*, Experimental characterization methods for thermal contact resistance: A review, *Applied Thermal Engineering* **130** (2018) 1530, https://doi.org/10.1016/j.applthermaleng.2017.10.163

39. H. Ding *et al.*, A review from fundamental research to device applications for graphene-based thermal rectifier, *DeCarbon* **4** (2024) 100048, https://doi.org/10.1016/j.decarb.2024.100048

40. X.-K. Chen *et al.*, A wave-dominated heat transport mechanism for negative differential thermal resistance in graphene/hexagonal boron nitride heterostructures, *Applied Physics Letters* **110** (2017), https://doi.org/10.1063/1.4977776

41. A. Joshi and C. Ramachandran, High-bias negative differential resistance effect in pure, doped and co-doped carbon nanotubes connected to boron nitride nanotubes, *Physica E: Low-Dimensional Systems and Nanostructures* **113** (2019) 1, https://doi.org/10.1016/j.physe.2019.04.021